World Academy of Science, Engineering and Technology
International Journal of Mechanical and Mechatronics Engineering
Vol:11, No:3, 2017

Magnetic End Leakage Flux in a Spoke Type Rotor Permanent Magnet Synchronous Generator

Petter Eklund, Jonathan Sjölund, Sandra Eriksson, Mats Leijon

***Abstract*—**The spoke type rotor can be used to obtain magnetic flux concentration in permanent magnet machines. This allows the air gap magnetic flux density to exceed the remanent flux density of the permanent magnets but gives problems with leakage fluxes in the magnetic circuit. The end leakage flux of one spoke type permanent magnet rotor design is studied through measurements and finite element simulations. The measurements are performed in the end regions of a 12 kW prototype generator for a vertical axis wind turbine. The simulations are made using three dimensional finite elements to calculate the magnetic field distribution in the end regions of the machine. Also two dimensional finite element simulations are performed and the impact of the two dimensional approximation is studied. It is found that the magnetic leakage flux in the end regions of the machine is equal to about 20 % of the flux in the permanent magnets. The overestimation of the performance by the two dimensional approximation is quantified and a curve-fitted expression for its behavior is suggested.

***Keywords*—**End effects, end leakage flux, permanent magnet machine, spoke type rotor.

I. Introduction

SPOKE-TYPE permanent magnet (PM) rotors are typically used with magnetic flux concentration. The magnetic flux concentration makes them useful when it is desirable for the air gap flux density to exceed the remanent flux density of the PMs. This can be the case either when a very high air gap magnetic flux density is needed, or when using low remanence PMs such as hard ferrite PMs.

The rapid price increase of neodymium-iron-boron PMs in 2011 [1] led to a large increase in research on alternatives, such as using ferrite PMs for instance. There are many studies of various variations of the spoke-type PM rotor. Most, however, choose to neglect the impact of end effects, whether in the form of end winding reactance or magnetic leakage flux. Those who do take the end effects into account do so by 3D finite element analysis [2], [3], which is time consuming, both to set up and run.

In this paper the magnetic field in the end regions is investigated, and an attempt to account for the impact of the end effects in a two dimensional approximation is made.

This work was carried out with funding from the Swedish Research Council, grant number 2012-4706 and within the StandUP for Energy strategic research framework. The Åforsk Foundation, grant number 12-295, is also acknowledged for contributing to this work.

J. Sjölund, S. Eriksson and M. Leijon are with the Division of Electricity, Uppsala University, SE-75237 Uppsala, Sweden (e-mail: Jonathan.Sjolund@Angstrom.UU.se, Sandra.Eriksson@Angstrom.uu.se, Mats.Leijon@Angstrom.UU.se).

P. Eklund is with the Division of Electricity, Uppsala University, SE-75237 Uppsala, Sweden (corresponding author, phone: +46-18-471-7256; e-mail: Petter.Eklund@Angstrom.UU.se).

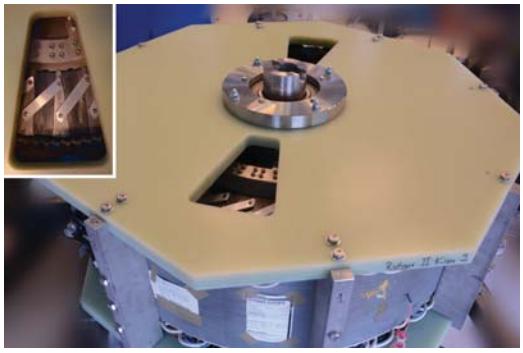

Fig. 1 Photograph of the generator used in the experimental work. Inset shows close up of pole ends and air gap. The octagonal end board is 1 m from side to side

TABLE I
Properties of the Investigated Generator

Parameter	Value	Unit
Rated speed	127	rpm
Rated power	12	kW
Number of poles	32	–
Number of slots per pole and phase	5/4	–
Stator inner diameter	760	mm
Air gap length (narrowest part, average for all poles)	6.6	mm
Stator stack length	224	mm
Rotor pole piece length	224	mm
PM size	$224^{+5}_{-0} \times 122 \times 38$	mm
PM material	Hard ferrite	–
PM remanence (measured average)	0.38	T

II. The Studied Machine

The machine used in the experimental work is a PM generator with a rated power of 12 kW at 127 rpm and is shown in Fig. 1.

The generator is a research prototype intended for use in an experimental wind turbine. It features a cable wound stator and have been retrofitted with a spoke type ferrite PM rotor. The design of the rotor used is described in [4] and the design of the stator and reminder of the original design is described in [5]. Some data about the design are given in Table I.

The PMs are slightly longer than the pole pieces in the axial direction. This overhang is to ensure that the PMs are as least as long as the pole pieces even when at the lower bound of the tolerance. All of this overhang occurs at the end shown in Fig. 1, at the other end both the PMs and the pole pieces have their faces flush against the aluminum rotor bottom plate.

The generator end boards are made from fiberglass

composite that is both non-magnetic and non-conductive.

The generator has previously been investigated with respect to manufacturing tolerances and it was found that the PMs have remanence below the tolerance [6]. The remanence measured in [6] is used in the calculations for this study.

III. Measurement of Magnetic Field in the End Regions

The magnetic field in the end region of the machine is measured at standstill using a Hall-probe. Measurements are made of the magnetic field component normal to the radial plane bisecting the PM, and of the axial component in the radial plane bisecting the pole. The locations of the measurements are indicated in Fig. 2.

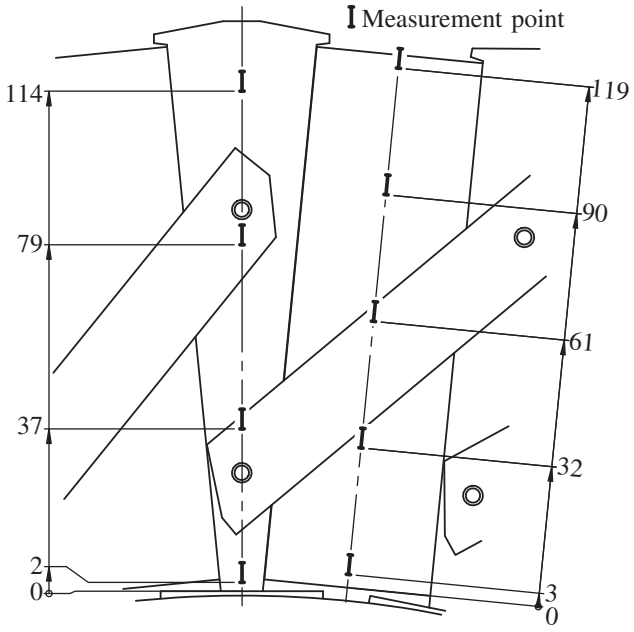

Fig. 2 Drawing of the generator end that shows the locations of the measurement point for one PM and one pole piece. The length of the measurement point marker indicates the width of the slot in the probe holder the Hall probe was inserted into. The width of the slot is $4.5\,\mathrm{mm}$. Over the pole (the set of points to the left) the probe is inserted into the holder from the side to measure the axial component of the field. Over the PM (the set of points to the left) the probe is inserted from the top to measure the tangential component of the magnetic field

The measurements are repeated for each pole and PM of the machine. A 3D-printed plastic probe holder is used to ensure that the probe is held in the same position relative to the pole or PM measured.

For each PM the tangential component of the magnetic field is measured at ten different positions. Five measurements each for two lines placed $13.25\,\mathrm{mm}$ and $31.25\,\mathrm{mm}$, in the axial direction, from the end surface of the pole pieces. For each pole the axial component is measured at four points on a line $25.25\,\mathrm{mm}$ from the end of the pole piece. These locations and directions are chosen to reduce the impact of probe misalignment. At the selected measurement points the field is expected to be mostly parallel to the measuring direction, because of symmetry.

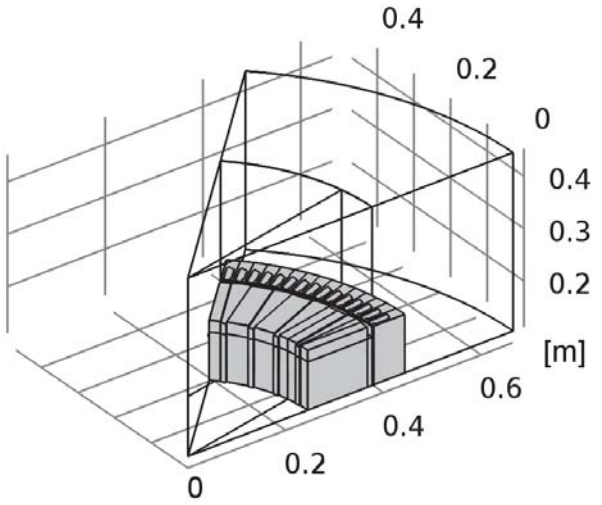

Fig. 3 The geometry of the simulated FEM-model. The size of the geometry is reduced by taking advantage of the rotational periodicity and mirror symmetry in the axial mid-plane

The radial component of the magnetic field near the end of the air gap is also measured. The probe is held in place by a fixture allowing it to be slid up and down in the axial direction of the machine. The fixture is mounted so that the field is measured about $2\,\mathrm{mm}$ from inner side of the stator and in front of a stator tooth. The rotor is positioned so that a rotor pole faces the stator tooth. This relative position between rotor and stator is also used in the simulations. The probe is then moved from about $20\,\mathrm{mm}$ outside the machine to $40\,\mathrm{mm}$ down into the air gap.

The Hall-probe instrument used is an FW Bell 5180 Gauss/Tesla Meter with an STD-18-0404 transversal probe. It is the same instrument that was used to measure the remanence in [6].

IV. Simulation of the Magnetic Field in the End Regions

The magnetic field in the end regions is simulated using the Finite Element Method (FEM). Scalar magnetic potential can be used since the machine is simulated at standstill and there are no free currents. Non-linear B-H-curves are used to model magnetic saturation of the iron in the rotor and stator. Periodic boundary conditions are used so that only a repeating 45° sector of the geometry needs to be simulated, reducing the computational effort. The lower half of the geometry is mirrored. This is done by removing the lower half and using magnetic insulation at the boundary, that is a zero normal component of the magnetic field on the boundary. The geometry of the 3D FEM-model can be seen in Fig. 3.

Most of the geometry of the machine is parametrically defined. A 2D approximation of the model is created by taking a cross section of the 3D model geometry. The magnetic field is then assumed to be in the plane of the cross section, and not to change in the axial direction. The remanence, $0.38\,\mathrm{T}$, and recoil permeability, 1.08, of the PM are taken from [6]. The 3D model is validated using measurements of the magnetic field in the prototype.

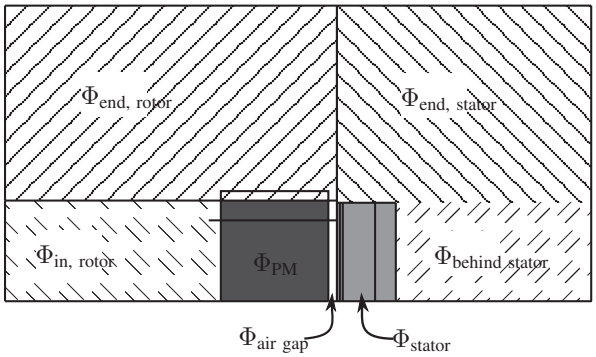

Fig. 4 The integration surfaces used in the 3D model to calculate the magnetic fluxes. In addition to the fluxes $\Phi_{\text{in, rotor}}$, Φ_{PM}, $\Phi_{\text{air gap}}$, Φ_{stator} and $\Phi_{\text{behind stator}}$, the 3D model includes the end magnetic flux leakages $\Phi_{\text{end, rotor}}$ and $\Phi_{\text{end, stator}}$. The axis of rotation is located at the left boundary of the figure

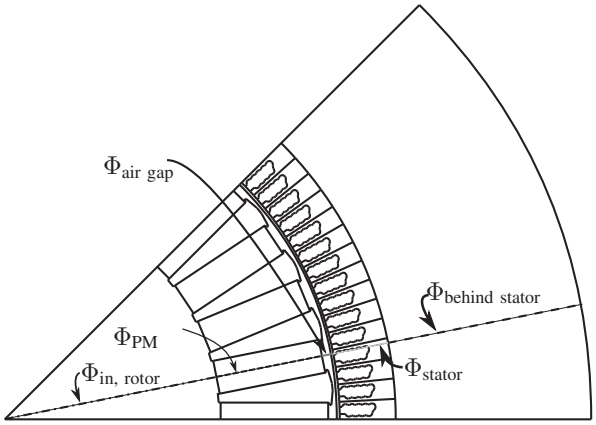

Fig. 5 The line segments used in the 2D model to form the integration surfaces used to compute the magnetic flux in different paths. The magnetic fluxes present in the 2D model are $\Phi_{\text{in, rotor}}$, Φ_{PM}, $\Phi_{\text{air gap}}$, Φ_{stator} and $\Phi_{\text{behind stator}}$.

To investigate the influence of the machine length, l_{machine}; air gap length, l_{ag}; width of the PM, across magnetization; and length of the PM, along magnetization, on the difference between the 2D approximation and the 3D model scaling factors are added. The scaling factors are then changed once at a time so that each of the lengths are scaled by a factor $2^{\pm 1}$ and $2^{\pm 1/2}$ if possible, otherwise the extreme and the square root of the extreme are used. When changing the geometry of the PMs the surrounding iron is changed correspondingly.

The radial plane bisecting the PM is divided into different flux paths, one for the magnetic flux trough the PM and the rest for the returning flux. The returning flux paths correspond to the useful flux passing the stator and different leakage flux paths. The integration surfaces used in the 3D model are shown in Fig. 4.

In the 2D model line segments multiplied by the machine length are used to form the integration surfaces. The integration line segments are shown in Fig. 5.

For both cases the component of the magnetic field normal to the integration surface is integrated to get the magnetic flux.

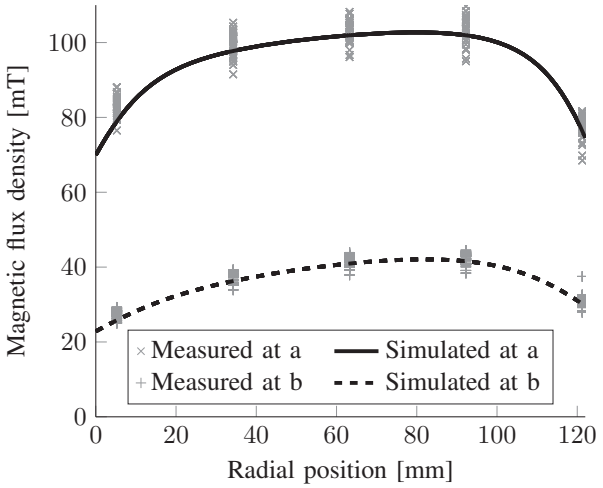

Fig. 6 Measured and simulated magnetic flux density normal to a radial plane bisecting the PM. The magnetic flux density is given along lines 13.25 mm (a) and 31.25 mm (b) above the end surface of the rotor pole pieces. Radial position is measured from the inner side of the PM as indicated in Fig. 2

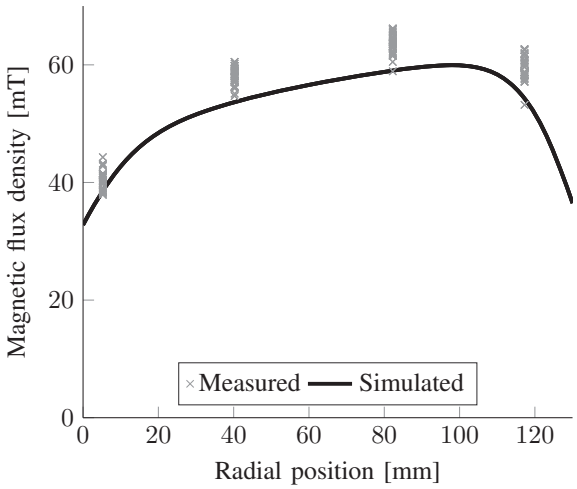

Fig. 7 Measured and simulated axial component of the magnetic flux density 25.25 mm over the end of the rotor pole pieces. Radial position is measured from the inner side of the pole piece as indicated in Fig. 2

V. The Magnetic Field in the End Regions

The simulations of the magnetic field are compared to measurements in Figs. 6 and 7. Fig. 6 shows the tangential component above the PM, at two different distances from the rotor end. Fig. 7 shows the axial component above the pole.

The components of the field tangential to the direction shown in the graphs are checked and confirmed to be small compared to the measured values.

The measurements of the tangential component of the magnetic field above the PM show good agreement with the simulation. The simulated field lies near the middle of the span of the measured values in all the measurement points. Some variation between poles is to be expected due to magnetic tolerances of the components; earlier investigation of the machine revealed some variation of PM remanence between poles [6].

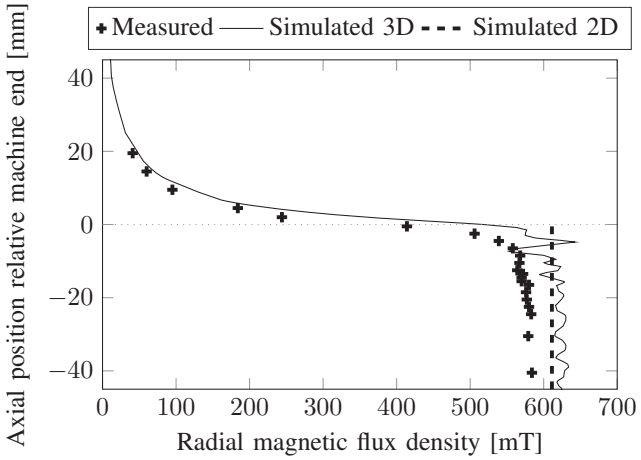

Fig. 8 The radial component of the magnetic field along a line starting in the air gap (y-axis less than zero) and extending out from the machine (y-axis larger than zero). The position in the plane of rotation is in front of a stator tooth facing a rotor pole. Simulation data is the average inside a ball of radius $1.5\,\mathrm{mm}$ to remove noise caused by the meshing of the geometry used by the FEM model

For the measurements of the axial component above the pole the simulation underestimates the field component. The simulated values are close to the lowest measured values. The field in this region is, however, very dependent on the location in the axial direction. The discrepancy is roughly equivalent to an error of $1\,\mathrm{mm}$ to $1.5\,\mathrm{mm}$ in axial position, or roughly the thickness of the Hall probe used for the measurements.

The radial component of the magnetic field in the air gap and some distance outside the machine end is shown in Fig. 8. Agreement is good considering there is some uncertainty in the position of the probe and rotor angle during measurement. The dent in the simulated magnetic flux density curve at around $-7\,\mathrm{mm}$ is most likely caused by a problem with the mesh.

Numerically computed field lines of the simulated magnetic field are shown in Fig. 9. The field lines shows that the axial component of the magnetic field grows toward the end of the machine. Further, it shows that the axial component mainly is present in the pole pieces, while the magnetic field in the PM is mostly in the plane of rotation.

When planning the measurement it was assumed that the magnetic field was mostly normal to the radial plane bisecting the PM, this assumption is confirmed by Fig. 9. The figure also support the assumption that the magnetic field in the end region is mostly axial in the plane bisecting the pole.

The simulated magnetic field in a radial plane bisecting a PM is shown in Fig. 10. The component of the magnetic field normal to the plane dominates, as expected from symmetry. The field outside the machine decays exponentially, which can be expected from a magnetic field when moving away from the sources.

The simulated magnetic field in a radial plane bisecting a rotor pole is shown in Fig. 11. The field lies mostly in the plane, and outside the machine end it is approximately axial over the pole piece, as expected from symmetry and confirmed by measurements. While the axial component of the magnetic field in the pole piece increases when moving

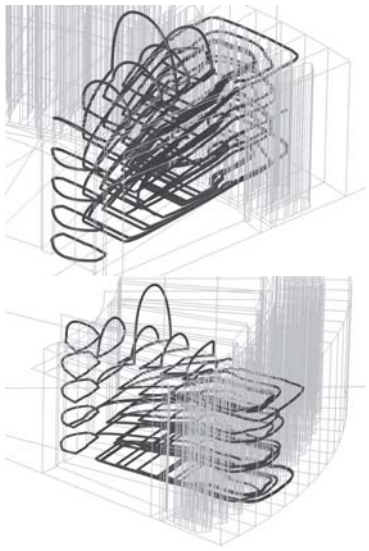

Fig. 9 Field lines of the magnetic field in the machine drawn as dark gray lines. The geometry is shown in lighter gray lines, the end of the machine is up in the figure, the bottom end is the mirror plane, and the boundary in the foreground is the periodic boundary. Two different views of the same set of field lines are shown

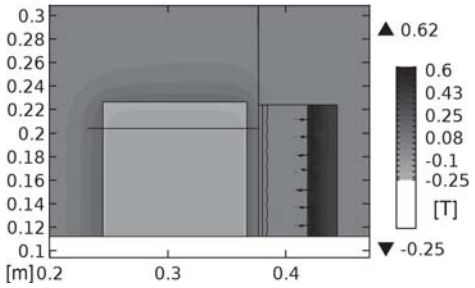

Fig. 10 Magnetic field in the radial plane bisecting a PM. Arrows are the components tangential to the plane, the normal component is given by the color scale. Scale on the arrow plot is $0.17\,\mathrm{T\,m^{-1}}$. The measurements presented in Fig. 6 are performed along lines corresponding to vertical coordinates $0.237\,\mathrm{m}$ and $0.255\,\mathrm{m}$. The stator is to the right and the PM in the center. The horizontal line close to $0.2\,\mathrm{m}$ is part of the simulation geometry to control the mesh. The lower edge is the mirror symmetry plane.

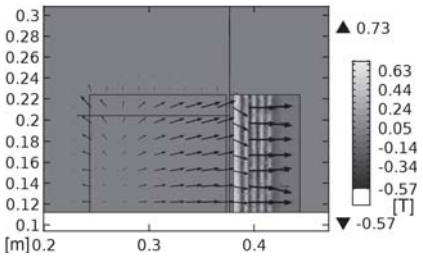

Fig. 11 Magnetic field in the radial plane bisecting a pole. Arrows are the components tangential to the plane, the normal component is given by the color scale. Scale on the arrow plot is $0.025\,\mathrm{T\,m^{-1}}$. The measurements presented in Fig. 7 are performed along a line corresponding to vertical coordinate $0.249\,\mathrm{m}$. The stator is to the right and the rotor pole in the center The horizontal line close to $0.2\,\mathrm{m}$ is part of the simulation geometry to control the mesh. The lower edge is the mirror symmetry plane

TABLE II
COMPARISON OF THE MAGNETIC FLUXES CARRIED BY DIFFERENT FLUX PATHS IN THE 2D AND 3D FEM MODELS FOR THE DEFAULT GEOMETRY

Magnetic flux [mWb]	2D	3D
Φ_{PM}	3.99	4.68
Φ_{stator}	2.87	2.73
$\Phi_{\text{air gap}}$	0.31	0.29
$\Phi_{\text{in, rotor}}$	0.83	0.75
$\Phi_{\text{behind stator}}$	3×10^{-4}	4×10^{-4}
$\Phi_{\text{end, rotor}}$	-	0.88
$\Phi_{\text{end, stator}}$	-	0.06

from the mid-plane to the machine end, the main change of the norm of the magnetic field is in the radial direction.

The total magnetic flux through the PM is $4.7\,\text{mWb}$, of this $58\,\%$ will cross the air gap and pass through the stator according to simulations. The end leakage flux is equal to $20\,\%$ of the magnetic flux from the PMs, making it the largest leakage flux. Another $16\,\%$ of the total flux through the PM will pass through the interior of the rotor and the last $6\,\%$ will pass between the poles in the air gap. Since the machine have a low length to diameter ratio it can be expected that the end leakage flux path will carry a large part of the total magnetic flux provided by the PMs.

VI. END EFFECT CORRECTIONS FOR 2D SIMULATIONS

The magnetic fluxes for the 3D and 2D simulations are compared in Table II. The 2D approximation removes the end leakage flux path, which is of significant permeance. The removal of this flux path mean that the PM sits in a magnetic circuit with lower permeance. This shifts the PMs working point on the BH-curve further from the B-axis, which corresponds to a smaller Φ_{PM}. The increased magnetic flux from the PM, and redistribution of magnetic flux from the $\Phi_{\text{in, rotor}}$ to the end leak paths reduces the difference in Φ_{stator} between the 2D and 3D case.

To compare the 3D and 2D simulations the ratio of Φ_{stator} for 3D over the same for 2D

$$\bar{\Phi}_{\text{3D/2D}} = \Phi^{\text{3D}}_{\text{stator}} / \Phi^{\text{2D}}_{\text{stator}} \tag{1}$$

where superscripts indicate 3D and 2D, respectively, is used. Using $\bar{\Phi}_{\text{3D/2D}}$ for the comparison between 3D and 2D is done because the magnetic flux through the stator reflects the induced voltage of the machine. Therefore $\bar{\Phi}_{\text{3D/2D}}$ should give the ratio of the induced voltages for 3D over 2D. The ratio $\bar{\Phi}_{\text{3D/2D}}$ can also be computed easily from a static simulation which is an advantage. One issue is how much of the stator cross section to consider carrying useful magnetic flux. Here the whole stator cross section is used when computing Φ_{stator}. This may include some of the slot leakage flux in Φ_{stator} but this inclusion should be approximately the same in both the 2D and 3D case, not affecting the comparison.

The ratio $\bar{\Phi}_{\text{3D/2D}}$ versus the relative change of the selected geometry parameters are shown in Fig. 12.

The machine length and air gap length show clear trends while trends of the length and width of the PM are inconclusive. A possible reason why the PM size parameters

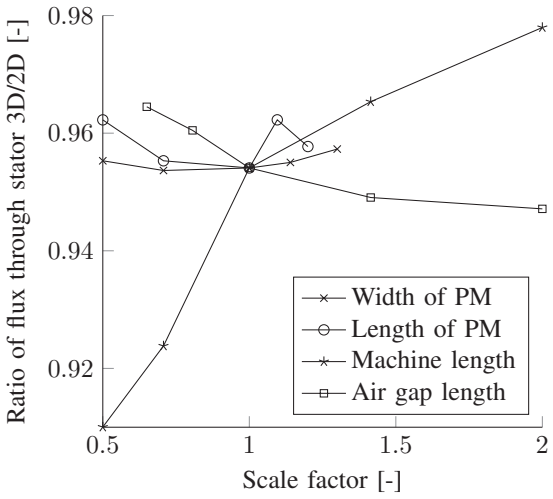

Fig. 12 Ratio of magnetic flux through stator computed by 3D FEM and 2D FEM for changes in selected geometry parameters. Width of the PM is across the magnetization and length of the PM is along the magnetization

show no clear trends for $\bar{\Phi}_{\text{3D/2D}}$ is that the possible variation of them are narrowly constrained geometrically. This prevents large changes in the parameter values without altering the topology of the rotor. This in turn makes it hard to tell the difference between modeling errors and changes in dependent values. Changes in the width of the PM give very little change in $\bar{\Phi}_{\text{3D/2D}}$ compared to what changes in the other parameters cause and only a very slight increasing trend. Changes of the length of the PM cause more change in $\bar{\Phi}_{\text{3D/2D}}$ but it appears highly irregular.

The value of $\bar{\Phi}_{\text{3D/2D}}$ asymptotically approaches unity as the machine length increases, which reflect a decreasing impact of end effects as the machine grows longer. For decreasing machine length the rate of change in $\bar{\Phi}_{\text{3D/2D}}$ grows more negative.

Using curve fitting techniques an approximation for $\bar{\Phi}_{\text{3D/2D}}$ in terms of machine geometry parameters can be found. The approximation is

$$\bar{\Phi}_{\text{3D/2D}} = \frac{l_{\text{machine}}}{l_{\text{machine}} + \frac{\pi D}{p} \tanh\left(\frac{l_{\text{ag}} p^2}{\pi^2 D}\right)\left(\frac{\pi}{p}\right)^{2/3}} \tag{2}$$

where p is the number of poles, D the diameter of the stator bore, l_{machine} the length of the machine and l_{ag} the length of the air gap. The approximation is compared to the simulation data in Fig. 13.

The fit is reasonable and the asymptotic behavior in l_{machine} is correct, vanishing at $l_{\text{machine}} = 0$ and approaching unity as l_{machine} grows large. Agreement is better for small l_{ag} than for large but this should not pose a problem as l_{ag} is relatively large for the size of the machine. It should be noted that (2) is not derived from first principles but fitted to a limited set of data points. A limitation of the dataset is that the ratio $\frac{D}{p}$ is not changed, reducing the generality of the obtained fit.

Once a value of $\bar{\Phi}_{\text{3D/2D}}$ is obtained, either by use of 3D FEM, (2) or other means, it can be used to apply corrections to a 2D FEM simulation. The simplest way to do this is

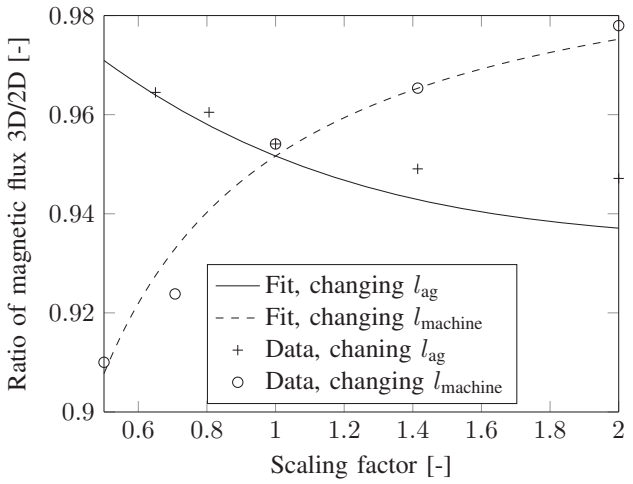

Fig. 13 Comparison of the approximation of $\bar{\Phi}_{\text{3D/2D}}$ given by (2) to the simulation data

to multiply the machine length by $\bar{\Phi}_{\text{3D/2D}}$ when computing induced voltage and inductance. A more complicated way is to adjust the remanence of the PM until $\Phi^{\text{2D}}_{\text{stator}} = \Phi^{\text{3D}}_{\text{stator}}$. The former is preferable both from a physical standpoint and a computational. The magnetic field component in the plane of rotation is slightly decreased in the 3D case compared to the 2D case but the norm of the magnetic field will be more or less the same due to the axial component which is not present in the 2D simulation. This means that the magnetic saturation of the steel is more accurately described by scaling the machine length.

VII. Conclusion

The magnetic end leakage fluxes in a spoke type rotor has been measured and simulated with good agreement. The magnetic end leakage flux in the studied machine is about one fifth of the total magnetic flux passing through the PMs and the largest leakage flux. It increase the permeance of the magnetic circuit, that increases the magnetic flux in the PM meaning that the impact on the main flux is reduced.

The relative impact of the end leakage flux decreases as the machine length increases and it decreases as the air gap length shrinks. To compensate a 2D simulation the machine length can be scaled by the ratio of magnetic flux passing through the stator for the 3D case over the 2D case. This ratio can either be obtained from the curve fitted expression (2) or from static 3D FEM with magnetic scalar potential at standstill.

References

[1] S. Eriksson and H. Bernhoff, "Rotor design for PM generators reflecting the unstable neodymium price," in *XXth International Conference on Electrical Machines*, Sept 2012, pp. 1419–1423.

[2] W. Kakihara, M. Takemoto, and S. Ogasawara, "Rotor structure in 50 kW spoke-type interior permanent magnet synchronous motor with ferrite permanent magnets for automotive applications," in *IEEE Energy Conversion Congress and Exposition*, Sept 2013, pp. 606–613.

[3] X. Ge, Z. Q. Zhu, J. B. Li, and J. T. Chen, "A spoke-type IPM machine with novel alternate airspace barriers and reduction of unipolar leakage flux by step-staggered rotor," in *IEEE International Electric Machines Drives Conference (IEMDC)*, May 2015, pp. 53–59.

[4] P. Eklund, S. Sjökvist, S. Eriksson, and M. Leijon, "A complete design of a rare earth metal-free permanent magnet generator," *Machines*, vol. 2, no. 2, p. 120, 2014.

[5] S. Eriksson, A. Solum, M. Leijon, and H. Bernhoff, "Simulations and experiments on a 12 kW direct driven PM synchronous generator for wind power," *Renewable Energy*, vol. 33, no. 4, pp. 674–681, 2008.

[6] P. Eklund and S. Eriksson, "Air gap magnetic flux density variations due to manufacturing tolerances in a permanent magnet synchronous generator," in *XXII International Conference on Electrical Machines (ICEM)*, Sept 2016, pp. 93–99.